INFLUENCE OF HEAT TREATMENTS ON FIELD EMITTERS ON Nb CRYSTALS

S. Lagotzky*, G. Müller, FB C Physics, University of Wuppertal, 42097, Germany
D. Reschke, A. Matheisen, DESY, 22603 Hamburg, Germany

Abstract

Systematic investigations of the influence of heat treatments on parasitic field emitters (1 nA) up to activation fields of 160 MV/m on high-purity Nb samples at temperatures between 122°C (24 h) and 400°C (2 h) are reported. Two large grain and two single crystal Nb samples with typical preparations (40 µm BCP, 140 µm EP and final HPR at DESY) were used. For all samples a significant increase of the emitter number density with increasing T up to 32 emitters/cm² at 400°C were obtained, the strongest of which emitted already at 40 MV/m. The dependency of the emitter number density on the insulating Nb_2O_5 layer thickness is discussed.

INTRODUCTION

Enhanced field emission (EFE) from particulate contaminations and surface irregularities is one of the main field limitations of the superconducting Nb cavities required for the ILC. Systematic investigations on large grain (LG) and single crystal (SC) Nb have revealed an exponential increase of the emitter number density N with activation field E_{act} and EFE at much lower onset fields E_{on} (1 nA) of activated emitters. This emitter activation can be caused either by high E_{act} partially combined with microdischarges or by heat treatments (HT) at temperatures T between 120 and 800°C [1]. In cavities EFE activation by high T may also arise due to enhanced RF losses of particulates which are thermally isolated from the cavity surface. Moreover, HT between 120 and 800°C are integrated in the usual cavity fabrication process [2].

Previous EFE measurements on polycrystalline [3,4] as well as LG and SC [5] Nb samples have shown, that a strong emitter activation occurs after HTs at 400°C with low $E_{on} \geq 40$ MV/m, and remaining particulates and surface defects were identified as emitters. Since the EFE activation is rather weak at 120°C, a decrease of the natural insulating Nb_2O_5 layer thickness due to HT has been suggested as main reason for their EFE activation [1]. Therefore, we have started more detailed systematic EFE measurements on LG and SC Nb samples before and after different HT between 120 and 400°C.

EXPERIMENTAL DETAILS

Measurement Techniques

For the systematic EFE measurements we have used a non-commercial ultra-high vacuum ($p \sim 10^{-9}$ mbar) field emission scanning microscope (FESM) as shown in Fig. 1 [6]. Flat samples up to 25×25 mm² can be investigated after surface tilt correction relative to the truncated cone anode (Ø = 300 µm) in order to achieve a constant gap Δz within ±1 µm for a typical (±5 mm) scan area. The FESM employs a PID-regulated power supply FUG HCN100M-10000 (10 kV, 10 mA) controlled by the EFE current as measured with an analog electrometer Keithley 610C or a digital picoammeter Keithley 6485. Non-destructive voltage scans V(x,y) for a limited EFE current (I = 1 nA) were performed with a resolution of 150 µm to localize emitters and to determine their N as function of E_{act} in reasonable steps (1 kV). Using the average Δz = 50 µm estimated from the long range optical microscope image, electric field maps E(x,y) up to 160 MV/m were derived.

For most emitters of each map, I(V) characteristics were locally measured up to 1 nA. The actual local field E_{on} was calibrated for each emitter as slope of a PID-regulated V(z) plot for 1 nA. Using the modified Fowler-Nordheim law [8]

$$I_{FN} = A\frac{S_{FN}\beta_{FN}^{\ 2}E^2}{\varphi\ t^2(y)}\exp\left(-B\frac{\varphi^{3/2}v(y)}{\beta_{FN}E}\right) \qquad (1)$$

the field enhancement factor β_{FN} and the emitting area S_{FN} can be calculated for a given work function φ. For simplicity, we have taken φ = 4eV (Nb), v(y) = t(y) = 1, A = 154 and B = 6830 for E in MV/m and I_{FN} in A.

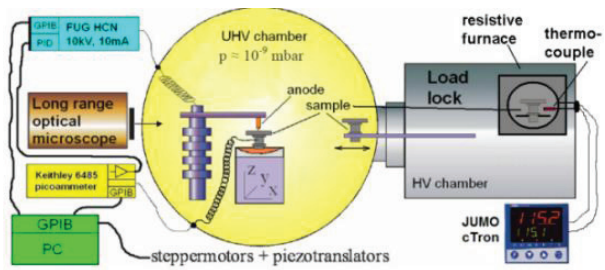

Figure 1: Schematic view of the FESM [7].

After FESM measurements the surface quality of the samples was investigated by means of a commercial optical profilometer (OP) with a lateral resolution of 2 µm as described elsewhere [9]. Further zooming into areas up to 98×98 µm² was achieved with an AFM in contact mode which can be positioned within ±2 µm of the OP results and has a lateral (vertical) resolution of 3 nm (1 nm). Using these results the linear and square roughness R_a and R_q of the surfaces can be calculated, and the geometric field enhancement factor β_{geo} of pronounced features can be estimated. Finally scanning electron microscopy (SEM) with energy dispersive x-ray analysis (EDX) was applied to search for the EFE origin and foreign materials at the emission site within a correlation accuracy of ±100 µm.

*s.lagotzky@uni-wuppertal.de

Copyright © 2013 by the respective authors

Heat Treatments

For HT of the samples a resistive furnace located in the load-lock of the FESM (Fig. 1) was used which provides temperatures T up to 1200°C under HV conditions (<10^{-6} mbar). T is measured with a thermocouple (Pt10Rh-Pt type S) and regulated by a commercial PID-controller (JUMO cTRON 04) within ± 1°C. The HT consist of a warm-up ramp from room temperature to the set point (≤ 6.3 °C/min), the annealing over time t and a natural cool-down phase, which can last up to 3h for T = 400°C.

In order to get useful steps after the usual cavity baking conditions (HT122), the required duration t of HT at different T can be estimated from calculations of the amount of produced oxygen atoms [10]:

$$C_{ox} \propto 1 - \exp(-k_{ox}(T) \cdot t) \quad (2)$$

The oxygen is released from the conversion of the natural insulating Nb_2O_5 layer with an original thickness of d_{ox} = 64 Å [11] into the semiconducting NbO_2 and finally into the metallic NbO with the overall reduction rate [10]

$$k_{ox} = A \cdot \exp(E_a / RT) \quad (3)$$

(A ≅ $3 \cdot 10^9$ 1/s and E_a ≅ 135 kJ/mol). C_{ox} was increased by one order of magnitude by choosing appropriate T and t until C_{ox} = 1 (HT325) with an additional HT at T = 400°C. XPS surface analysis of anodized and heated Nb samples [11], however, show that even at C_{ox} = 1 a thin Nb_2O_5 layer is still present on top of the Nb surface. In table 1 the graphically from [11] interpolated d_{ox} values are compared to the C_{ox} values. Probably this discrepancy can be explained by an incomplete diffusion of the produced oxygen atoms out of the oxide layer.

Table 1: Parameters of HT, values of C_{ox} calculated with (2) and (3), and d_{ox} taken from [11].

HT	T [°C]	t [h]	Warm-up time [h]	C_{ox}	d_{ox} [Å]
Initial	22	672	-	$1.57 \cdot 10^{-8}$	64.0
HT122	122	24	3	$3.64 \cdot 10^{-4}$	45.0
HT150	150	12	1	$2.76 \cdot 10^{-3}$	39.4
HT175	175	9	1	$1.75 \cdot 10^{-2}$	34.5
HT200	200	8	1	0.101	30.0
HT250	250	10	1	0.971	20.7
HT325	325	6	1	1.000	11.0
HT400	400	2	1	1.000	6.6

Samples

We have used two LG and two SC Nb (RRR > 250) samples with a diameter of 28 mm welded to a support rod. The samples were polished at DESY in two steps: 1. buffered chemical polishing (HF (48%): HNO_3 (65%): H_3PO_4 (85%), 1:1:2) up to 40 µm and 2. electropolishing (HF (40%): H_2SO_4 (98%) 1:9) up to 140 µm. Finally they were high pressure rinsed with ultrapure water, covered with dry-ice-cleaned protection caps (Fig. 2), sealed in plastic bags in a cleanroom class ISO5 and transported to Wuppertal. The protection caps were not removed until the samples faced at least high-vacuum conditions in the load-lock of the FESM and also used during transport to other measurement systems. The samples have two marks on the edge for correlated positioning in FESM, OP and SEM.

Figure 2: Nb sample with protection cap.

RESULTS AND DISCUSSION

Surface Quality

Survey scans (OP, 25×25 mm², 25 µm lateral res., (Fig 3a) showed that the surface of the samples is flat (±2 µm) in the central areas (1 cm²). The mean roughness of the samples in these areas was R_a = 83 nm (R_q = 103 nm) for the SC Nb samples and R_a = 117 – 205 nm (R_q = 149 – 248 nm) for the LG Nb samples depending on the grain orientation. The AFM measurements (98×98 µm², 10 nm lateral res.) showed R_a = 8 nm (R_q = 10 nm) for SC Nb and R_a = 7 – 11 nm (R_q = 9 – 14 nm) for LG Nb. High resolution OP in small (1 mm²) selected areas (Fig. 3b) showed only few surface defects with low $\beta_{geo} \leq 6$, e.g. strings of small pits as residues of scratches, and AFM profiles at the grain boundaries revealed only $\beta_{geo} \leq 4$ (Fig. 3c). According to (1), geometrically caused EFE from these samples should not arise up to field levels of about 300 MV/m.

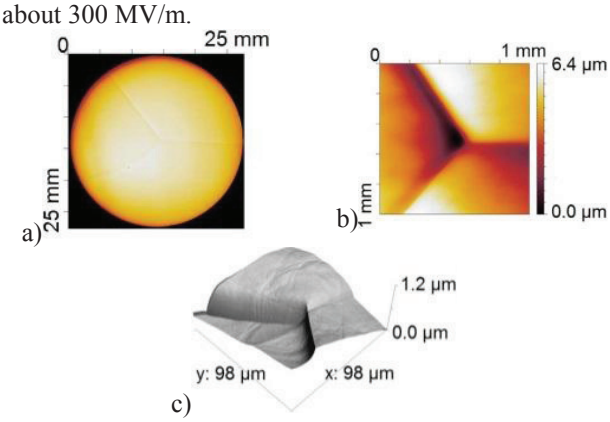

Figure 3: (a) OP profile of LG sample (25 µm lateral resolution), (b) OP (2 µm lateral res.) and (c) 3D-AFM profile (10 nm lateral res.) of the grain junction.

EFE Statistics of HT Activated Emitters

The EFE of all samples was investigated in the central areas of 1 cm^2 before and after each HT as listed in table 1 (HT325 only on one LG, HT250 & HT400 only on two LG and one SC). For the best sample shown in Fig. 4, no field activation was observed initially up to 160 MV/m, but a clear increase of N with increasing T demonstrates strong HT activation of emitters. The other three samples showed already few emitters at 100 MV/m before HT, but similar strong HT-activation effects, too. A dependency of the EFE on the grain boundaries or the crystal orientation of Nb could not be observed.

Copyright © 2013 by the respective authors

ISBN 978-3-95450-143-4

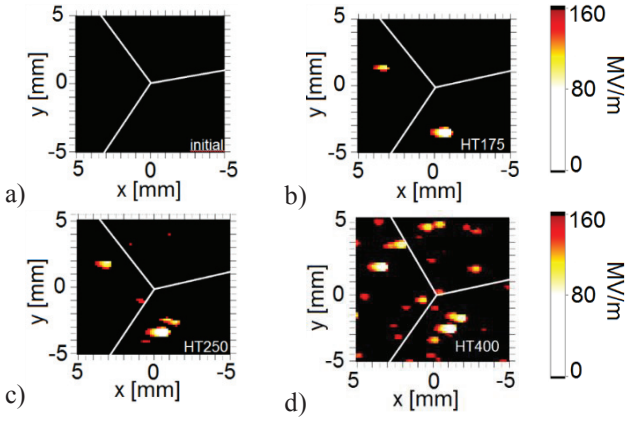

Figure 4: Field maps up to 160 MV/m of one LG sample at initial status, after HT175, HT250 and HT400.

In order to reduce the statistical error, the total number density of field- and HT-activated emitters on all four samples is shown in Fig. 5a. Obviously $N(E_{act})$ increases exponentially within error bars after all HT. The monotonous shift to higher N with T indicates that emitters on an annealed surface can be already activated at lower E_{act} than on initial Nb surfaces. Moreover, HT lead to emitters with E_{on} down to 40 MV/m (Fig. 5b), which are relevant for the ILC (E_{acc} = 31.5 MV/m, E_{peak}/E_{acc} = 2).

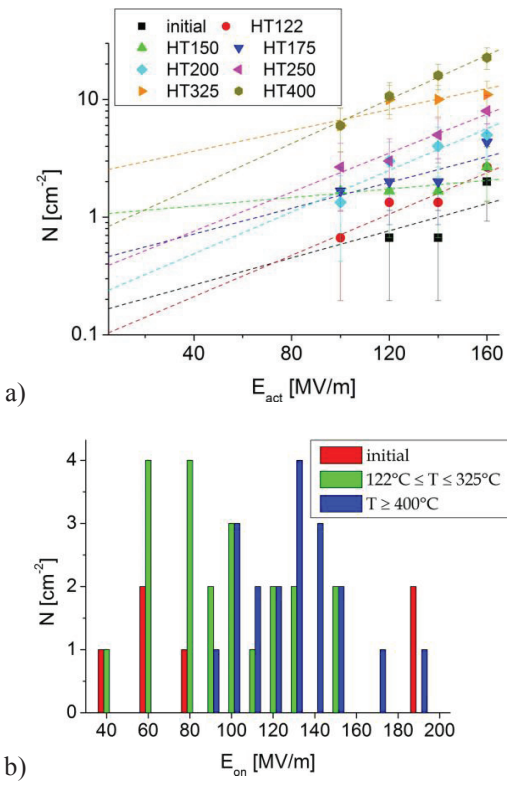

Figure 5: (a) $N(E_{act})$ after each HT with exponential fits (least square) and (b) histogram of $N(E_{on})$ for field activated emitters, emitters activated after HT122 - HT325, and emitters activated additionally by HT400.

In Fig. 6a, the number density of emitters activated by each HT (N_{HT}) increases until C_{ox} = 0.975 (HT250), but a further raise of N_{HT} can be observed until HT400, which would demand a second activation process. In contrast, correlating N_{HT} with d_{ox} from table 1 (Fig. 6b) leads to a monotonous decrease with oxide thickness. Moreover it seems that the difference between E_{act} and E_{on} becomes smaller for HT400 (Fig. 5b). Therefore, higher T or longer annealing times might lead to an activation of all potential emitters at their final E_{on}.

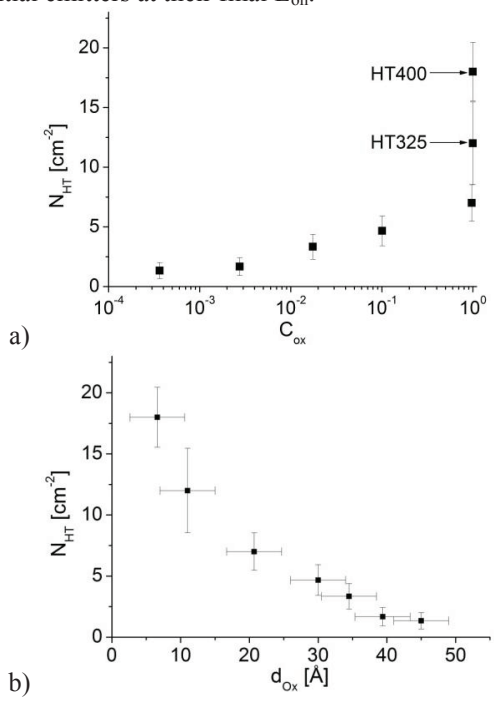

Figure 6: N_{HT} plotted against d_{ox} (a) and C_{ox} (b).

Single Emitter Characteristics

SEM investigations of the 10 strongest emission sites selected from all field maps revealed 30% surface defects, 30% particulates and 40% destroyed or unidentified emission sites. EDX in regions with particulates and destroyed emitters showed W (probably from the anode), Al and Nb.

Surface defects mostly showed a FN-like I-V curve, often with nearly parallel slopes after different HT (Fig. 7). The resulting FN parameters are reasonable for this feature but differ significantly from the calculated β_{geo} = 6 resulting from the AFM profile. It is remarkable that E_{on} of this emitter varies non-monotonously with d_{ox} and the current is most unstable after HT200 and HT250. This reflects a rather complex structure of the remaining oxide at this defect.

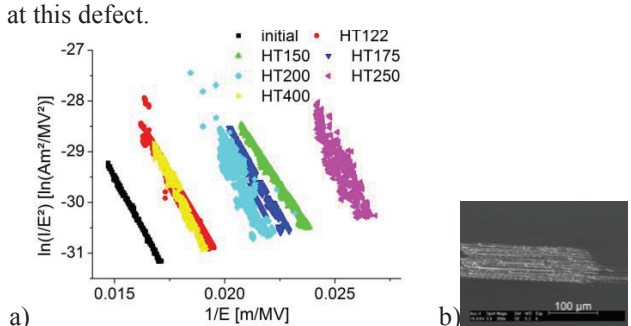

Figure 7: (a) FN-like EFE (β_{FN} = 62 - 83, S_{FN} = 10^{-5} - 10^{-2} µm²) of a surface defect (b).

Copyright © 2013 by the respective authors

In comparison, particulates like the one shown in Fig. 8 often reveal much more unstable IV-curves, which result in unreasonable FN parameters (e.g. $S_{FN} = 10^{11}$ km²). Therefore, metal-insulater-metal or resonant tunnelling emission models should be considered for such effects [12].

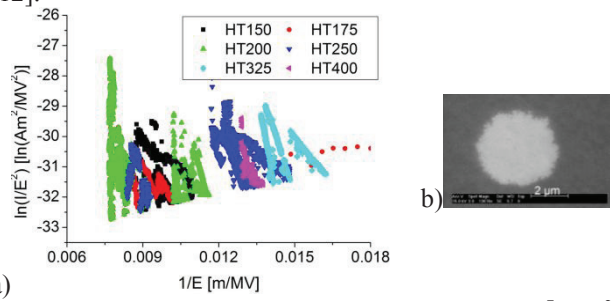

Figure 8: (a) unstable EFE (β_{FN} = 5 - 140, $S_{FN} = 10^{-7} - 10^{29}$ µm²) of a melted Al particulate (b).

CONLCUSIONS AND OUTLOOK

The HT of LG and SC Nb leads to activation of remaining particulates and surface defects due to the dissolution of the natural insulating Nb_2O_5 layer. Activated surface defects show FN-like EFE with reasonable β_{FN} and S_{FN} values, which are difficult to be derived from AFM profiles and SEM images. Activated particulates reveal unstable EFE and other mechanism.

Air exposure (or anodizing) of the surface might deactivate such emitters. Furthermore high current processing or ion impact of emitters should be investigated.

ACKNOWLEDGMENTS

Acknowledgements are given to Dr. A. Navitski for detailed discussions, Dr. R. Heiderhoff for access to SEM facility at FB E of University of Wuppertal, to N. Steinhau-Kühl for EP and to J. Ziegler for help with HPR treatment at DESY. The work is funded by Helmholtz-Allianz "Physics at the Terascale" and BMBF project 05H12PX6.

REFERENCES

[1] A. Navitski et. al, subm. to Phys. Rev. ST – Accel. Beams 2013.
[2] D. Reschke et al., Phys. Rev. ST – Accel. Beams 13, 071001 (2010).
[3] Ph. Niedermann et. al, J. Appl. Phys. 59 (1986).
[4] E. Mahner, Part. Accel. 46, 67 (1994).
[5] A. Dangwal, G. Müller, D. Reschke, X. Singer, Phys. Rev. ST – Accel. Beams 12, 023501 (2009).
[6] D. Lysenkov, G. Müller, Int. J. Nanotechnol. 2, 239 (2005).
[7] A. Navitski, PhD thesis, Univ. Wuppertal (2010).
[8] R. G. Forbes, J. Vac. Sci. Technol. B 17, 526 (1999).
[9] see contribution TUP093, this conference.
[10] G. Ciovati, Appl. Phys. Lett. 89 (2006), 022507.
[11] A. Dacca et. al, Appl. Surf. Sci. 126 1998. 219–230.
[12] R. V. Latham, "High Vacuum Insulation: Basic Concepts and Technological Practice," Academic Press: London, (1995).

Copyright © 2013 by the respective authors

ISBN 978-3-95450-143-4